Numerical Investigation on Performance of Gas Turbine Blade Effects of Simulation Models and Blade Geometry

Heng Hu, Narmin Hushmandi, Magnus Genrup

Energy Science department, Lund University, Box 118, 22100 Lund, Sweden
heng.hu@energy.lth.se

Abstract

With a significant impact on turbomachinery blade performance, surface curvature distribution becomes one of the essential factors in the design of high-efficiency blades. This study focuses on applying computational fluid dynamics (CFD) to evaluate turbine rotor blade performance. The main aim is to analyze the influence of incidence and geometry shape on the performance of a gas-turbine blade in two dimensions. To achieve this, an investigation was conducted to identify a suitable turbulence model for this case, with two turbulence models combined with two different solvers explored in ANSYS Fluent: Realizable k-ε model in pressure and density based solver; k-ω shear stress transport (SST) model in pressure and density based solver. The blade total pressure loss across different blade exit Mach numbers is the comparison factor, with validation against experimental data. Subsequently, the chosen pressure-based k-ω SST model mode is used to study the performance of various air inflow incidence angles and compare two different blade geometries. In this paper, two geometries, Geometry 1 and Geometry 2, were designed by setting two different exit blade angles, β_2=79.5° and β_2=70° respectively, while the inlet blade angles have the same value, β_1=48.8°. Furthermore, the effect of varying air inflow incidence angles between -48.8° and 10° on the blade performance distribution is also investigated. Within the studied range, the inflow incidence angle of 10° is found to have the best performance in terms of turbine work output. On the other hand, the blade performance of Geometry 2 appears superior to Geometry 1.

1. Introduction

The blade geometric profile is designed to determine the efficient aerodynamic performance. Some principal aerodynamic objectives of a turbine blade design are: the blade angles at the inlet and exit must be correctly matched to the fluid flow angles; the throat area determines the flow capacity and must be sized correctly. Besides, Blade surfaces curvature and changes in curvature should be limited, consistent with the necessary turning of the flow in blade passage. So the blade design plays an essential role in the full design process. In turbomachinery, quality blade design is an integral element to efficient aerodynamics (Lebele-Alawa et al., 2008), which can affect the entire blade row's performance, affecting the overall machine efficiency (Fast M et al., 2009). In particular, blade curvature distribution has been shown to influence boundary-layer characteristics, determining blade losses and efficiency (Korakianitis et al., 1993).Even though the field of blade curvature is relatively mature, the potential benefits of sizeable industrial cost-savings and environmental impact from even a tiny efficiency improvement have been sustaining the keen interest in work in this area.

The turbine portion in gas turbine systems extracts work from the combusted gases to power the compressor stages and drive other loads. As such, considerable effort has been poured into turbine blade research to attain maximum extraction of the valuable work output. Additionally, to further push the upper bound of turbine efficiency, much research has been done on limiting flow separation that contributes to decreases in work output (Korakianitis T P. et al., 1989) Unsurprisingly, the surface curvature of the blade determines its loading distribution, forming a crucial factor in controlling flow separation (Nemnem et al., 2014). In further detail, a smooth curvature distribution at the blade leading edge has been found to prevent the formation of separation bubbles, thus suppressing the flow separation (Song Y et al., 2014).

This paper considers how blade parameterization affects profile losses and loading diagrams in a numerical approach, including blade angles, incidence, etc. It is worth highlighting that one main objective of the paper is to explore and compare different numerical models against a set of experimental data to identify a suitable model for this application. Designing a turbine blade geometry typically starts from a one-dimensional approach before moving on to two-dimensional (2D) and eventually developing into 3D in the final phase. This paper involves the 2D round, which is practical

regarding the scope and computational cost. Coupled with the computationally economical RANS models, the approach reflects a common means adopted in industries to offer a quick blade diagnostic tool for trend studies. The selected RANS model is subsequently applied to the turbine blade design to relate the modified parameters to the selected blade performance indicators.

In addition, this paper also seeks to demonstrate the key role of CFD in both industry and academic research for turbine blade design. CFD today is an indispensable part of blade design as it provides a performance evaluation for a particular geometry. It can also be used to pick out the blade locations requiring modifications, forming an iterative part of the design process to optimize surface geometry and loadings.

2. Numerical Simulation

For this research, the fluid flow parameters, e.g., velocity magnitude, pressure, temperature, and Mach number, around the turbine blade will be simulated using numerical methods. Two turbine blade geometries with different exit blade angles were generated to examine the influence of blade geometry. The ANSYS ICEM CFD was used to mesh the geometry. The commercial CFD software, ANSYS Fluent, is used for solving and post-processing.

2.1. Turbine Blade Geometries

This paper aims to find the influence of different solvers, incidence angle, and shape of turbine blades. For simplification of simulation cost, 2D geometries are selected for this study. Figure 1(a) shows the schematic diagram of blade section parameters. AxCent of Concepts NREC design tools software provides a good way to generate the geometries by determining the blade section parameters (such as inlet/exit blade angles, stagger angles, gauge angles, wedge angles, chords, and pitch).

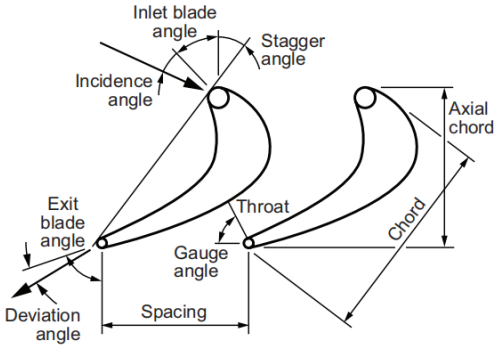

(a) Schematic diagram of blade section parameters

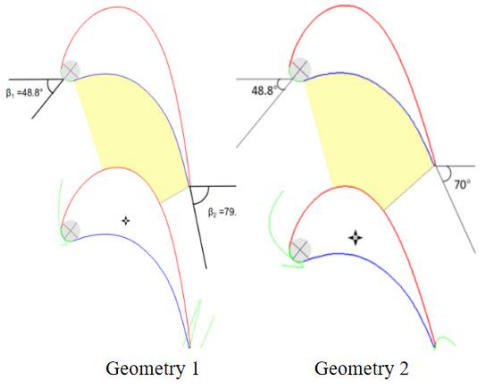

(b) Schematic of blade sections for two geometries.

Figure 1: Schematic of the 2D blade.

In this research, two blades were designed by setting two different β2: exit blade angle, β2=79.5°, and β2=70° respectively, while the β1: inlet blade angle have the same value, β1=48.8°. The two blade geometries are shown in Figure 1(b). Geometry 1 is a reference blade profile of Atlas (Mee D J et al., 1992). Since Geometry 1 has experimental results, most of the simulations in this paper are based on Geometry 1. In order to study the influence of blade geometric parameters on blade performance, based on Geometry 1, modifications are done to the exit blade angle to obtain Geometry 2. The remaining important blade parameter values of Geometry 1 and Geometry 2 are shown in Table 1.

Table 1: Blade parameters.

Parameters	Geometry 1	Geometry 2
Chord (m)	0.0474	0.0474
Stagger Angle(°)	-37.8	-29.8
Pitch/Chord	0.7593	0.7597
Axial Chord (m)	0.03745	0.0411

The Normalized curvature distribution of the two geometries generated in AxCent showing in Figure 2, which shows that, in the two cases, the blade curvature is continuous and smooth. The blade curvature distribution of the pressure side for the two geometries differs, while the blade curvature distribution on the suction side coincides.

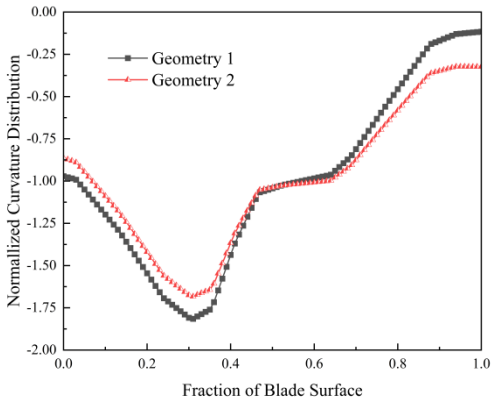

(a) Pressure Side

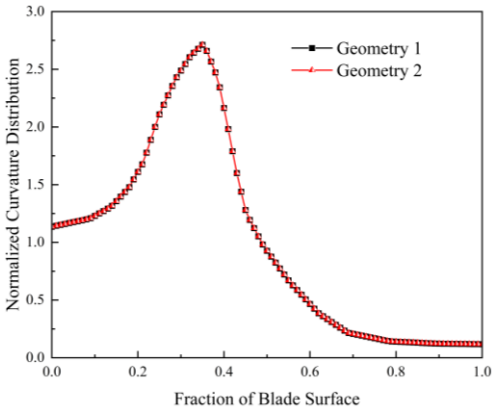

(b) Suction Side

Figure 2: Curvature distribution of the 2D blade sections for two geometries.

2.2. Mesh Generation and Boundary Conditions

The computational domain of fluid is divided into three parts: the upstream and downstream domains and the blade domain. The computation domain is extended upstream and downstream to achieve a fully developed flow. The inlet of the numerical domain is extended 0.8 times axial chord of the blade upstream of the blade leading edge, and the exit is extended 1.25 times the axial chord downstream of the blade trailing edge. Four types of boundary conditions are presented to solve a blade cascade: wall, periodic, inlet, and outlet (Moshizi S A et al., 2014). Using the periodic boundaries for the blade cascade is common in CFD to reduce the computational domain size and thus decrease the time and memory cost for processing (M. Mahmoudi et al., 2005), so just one blade passage simulated in all simulations. For the inlet and out boundary conditions, pressure-inlet and pressure-outlet are adopted, respectively. No-slip condition is used for the blade wall. The values of the boundary conditions applied to the cases are presented in Table 2.

Table 2: Boundary conditions.

Parameter	Value
Inlet/Outlet Total Temperature	1046(K)
Inlet Absolute Total Pressure	211325(Pa)
Outlet Absolute Static Pressure	126325(Pa)
Outlet Mach Number	0.7-1.1

With good quality of the structured mesh, using a higher-order discretization scheme, the solver solution would have a higher convergence rate and precision. Therefore, the software ICEM CFD was used to generate the structured grids for calculation domains around the blade surface. Figure 3 shows the meshes of Geometry 1 employed in the computational domain. The whole grid was structured with an O-H type of mesh, using the O-type mesh around the blade and H-type everywhere else. The meshes are refined for the near-wall treatment and are expected better to handle the complex turbulent flow around these areas and enhance computational accuracy. The first layer grid near-wall is 0.002 mm, and the y+ value is around 1.

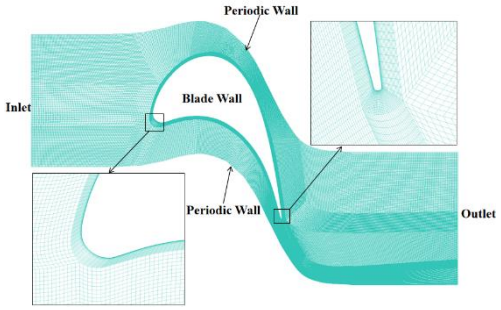

Figure 3: Numerical domain and mesh for the analysis of the geometry 1.

2.3. Grid Independence Study

A mesh independence analysis was done using various mesh densities to study the effect of grid resolution on the accuracy of numerical results. For this purpose, the grid resolution was increased until the blade total pressure loss had no significant variations.

This paper uses the total pressure loss coefficient to characterize the blade total profile loss. The definition of the total pressure loss coefficient:

$$Y_p = \frac{p_{01,in} - p_{02,out}}{p_{01,in} - p_{1s,in}} \quad (1)$$

Where $p_{01,in}$ represents the blade inlet total pressure, $p_{02,out}$ is the mass-weighted average total pressure at the blade section where extended 0.8 times the axial chord downstream of the blade trailing edge.

Nine grid sizes in the range of 5000 to 134 000 structured cells are evaluated. Figure 4 illustrates the variations of blade total pressure loss for the different grids. Due to the importance of computational efficiency, the mesh with 114 400 structured cells was chosen for Geometry 1; Geometry 2 has meshed with the same method, and the number of grids is comparable at 118 650 structured cells.

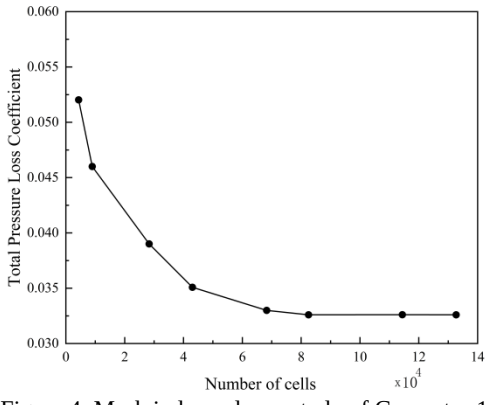

Figure 4: Mesh independence study of Geometry 1

2.4. Solver Settings

The governing equations for viscous compressible fluid are the continuity, Navier-Stokes momentum, and state equations. The equations are discretized with the finite volume method. Firstly, four different RANS models in Fluent - namely the Pressure-based k-epsilon method, Pressure-based SST k-ω method, Density-based Realizable k-ε method, Density-based SST k-ω method were used to solve the discretized equations. For the spatial discretization of pressure-based solver cases, the second-order scheme is used for pressure, and the second-order upwind scheme is used for momentum and turbulent kinetic energy terms. For the spatial discretization of density-based solver cases, the second-order upwind scheme is used for flow and turbulent kinetic energy terms. Besides, ideal gas model has been chosen because the physical fluid is a compressible fluid. Turbulence is chosen to be modeled using the Realizable k-ε and SST k-ω models due to the corresponding theoretical strengths in providing realistic results and superior performance for complex flows (like adverse pressure gradient and separated flows), respectively. The convergence of the solution is monitored by checking the residuals of the numerically solved governing equations, which use the absolute scale of residuals to converge until 1E-6.

In Fluent, the pressure-based solver is developed from the original separate solver, which solves the momentum, pressure correction, energy, and other scalar equations in sequence, such as the turbulence equation. Unlike before, the pressure-based solver also adds a coupling algorithm, which can be freely switched between the separation and coupling solutions. The coupling solution is to solve the aforementioned momentum and pressure correction simultaneously and then solve energy, component equations, and other scalar equations, such as Turbulence equations, etc., which have fast convergence speed but require more memory and calculation.

The difference between Pressure-based and Density-based: First, the pressure-based solver was mainly used for the solution of low-speed incompressible flow, while the density-based method was mainly designed for high-speed compressible flow, but now both ways have been extended to solve a large flow velocity range method. Second, the density-based solver was developed from the originally coupled solver. It simultaneously solves the continuity, momentum, energy, and component equation, then solves the turbulence and scalar equations. As a result, the density-based solver has a fast convergence speed and requires more memory and calculation time than the pressure-based solver!

As a result, the density-based solver is expected to take longer computational time per iteration. According to observation, for the studied Geometry 1, the density-based simulations took significantly longer to run and converge. The coupled algorithm is used for the pressure-based solver because of its higher accuracy. As the simulation is 2D and the grid resolution is not large, the trade-off in computational time is insignificant.

2.5. Model Validation

The experimental results of Atlas, involving the same blade design as Geometry 1, were used to validate the numerical solutions. The blade profile loss against different Mach numbers was profiled in the actual experiment. The inlet airflow direction specification method was set to be normal to the boundary, corresponding to an incidence angle of -48.8°. Additionally, the specification method for both inlet and outlet boundary conditions was based on turbulence intensity and turbulence viscosity ratios of 5% and 10, respectively. Different exit Mach numbers were obtained by adjusting the outlet pressure value.

Figure 5 shows the numerical blade losses across various exit Mach numbers found via the four model-solving cases close to experimental data. The models are pressure-based SST k-ω, density-based SST k-ω, pressure-based Realizable k-ε, and density-based Realizable k-ε. Although the numerical data do not overlap entirely with the experimental ones, the differences are within a reasonable range. The changing trend of the experimental and simulated structures is basically the same and have some slight difference. The plotted loss coefficients are for exit Mach numbers between 0.7 to 1.1. It is seen from the plot that, up to a specific exit Mach number (Ma=0.9), the total pressure losses are low. However, after Ma=0.9, the total pressure loss increases rapidly. The sudden increase is due to the appearance of shocks inside the blade channel. As the exit Mach number continues to grow to about 1.05, the simulation results show that the total pressure loss increases slowly with the exit Mach number, while the experimental results still increase significantly with the increase of the exit Mach number.

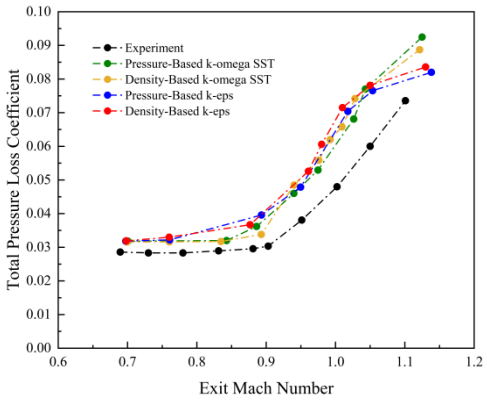

Figure 5: Comparison between numerical and experimental blade profile loss for Geometry 1.

The differences may have come from the following reasons. Firstly, the compressibility of air and the capture of shock waves in the simulation calculations may still differ from the actual problem; some factors, like the turbulent vortex in 3D space and dissipation in the third direction, cannot be captured by the 2D simulations in this research. Secondly, applying constant static pressure at the outlet affects the total pressure loss values. Besides, the empirical data measurement position and statistical approach may differ from the data collection of our numerical approach. Finally, this study is mainly on a transonic turbine blade, with exit Mach number ranging from about 0.7 to 1.1, for which it is notoriously difficult to get a precise solution with RANS models.

Similarly, the differences between the four cases are also slight. The data sets for density-based and pressure-based SST k-ω models are close to each other, while the density-based and pressure-based Realizable k-ε models also have a similar phenomenon. According to the literature (Corriveau D et al., 2007), the profile loss will vary slowly for high Mach numbers, which also can be observed in our current numerical results. When the Mach number is above almost 1.05, the density-based and pressure-based Realizable k-ε model has less variation than the SST k-ω models. So in terms of growth trend, the SST k-ω model is closer to the experimental growth trend than the Realizable k-ε model.

3. Results and Discussions

3.1. Comparison across Models

Before further research on this turbine blade, some variables, like Mach number, pressure, obtained in the model validation section were identified as key parameters. In addition, comparing the differences caused by different model-solver cases is also critical. Using geometry 1, we have done some simulations to explore the influence of model and solver selection. This study analyzes the conditions of different outlet Mach numbers 0.76 and 1.1, as shown in Figures 6-11. The most apparent difference between these two cases is the observation of shock waves. When the outlet Mach number is 1.1, the shock wave is obvious in all four models, as seen in Figure 6 and 7, while the flow field of four models is subsonic when the outlet Mach number is 0.76, as shown in Figures 9 and 10.

Figure 6 shows the contour of the exit Mach number of 1.1 under the same turbulence models with different solvers. Specifically, the density-based and pressure-based Realizable k-ε models have similar Mach number distributions, including the value range and position of the shock wave, while the density-based and pressure-based SST k-ω models capture a more severe shock. As it is seen from zoom-in figures, near the suction side of the outlet blade wall under the same solver, the SST k-ω model shows a better distribution of the reflected oblique shocks and expansion waves near the blade wall. Theoretically, the Realizable k-ε model might face inaccuracies for complex wall-bounded flows, such as predicting the early onset of flow separation or the inability to accurately capture turbulent shock wave-boundary layer interaction. Thus SST k-ω might be more reliable in this respect. The Mach number around the trailing edge of the turbine blade is small, which means the velocity is small, resulting from some adverse flow decrease in kinetic energy.

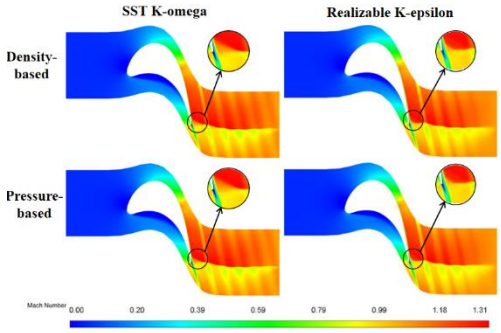

Figure 6: The Contour of Mach number of four models with exit Mach number 1.1.

Figure 7 and 8 show the contour of static temperature and total pressure of four models, respectively. Besides, in both figures, the 'inclined strip' near the outlet part is caused by the blade wakes, and the 'strips' are caused by other turbine blades present with the periodic boundary condition selection.

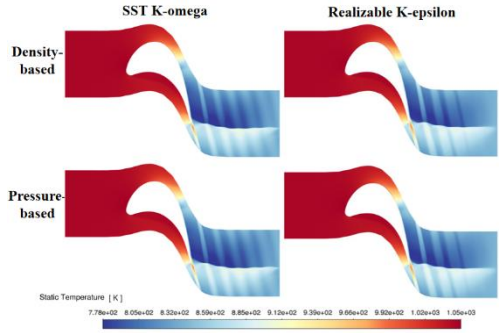

Figure 7: The static temperature of four models with exit Mach number 1.1.

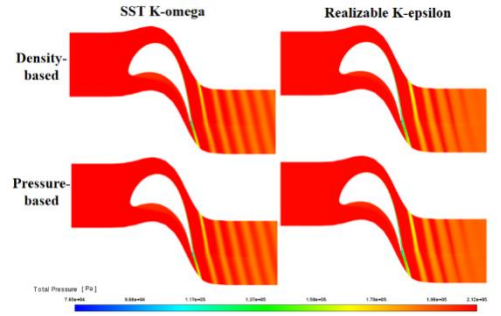

Figure 8: The Total Pressure of four models with exit Mach number 1.1.

As the outlet Mach number was decreased to 0.76, the entire flow field becomes subsonic, as shown in Figures 9. The maximum Mach number changed from about 1.31 to 0.85. Besides, the Mach number in the blade's trailing edge is more uniform, and there is no shock wave in the field.

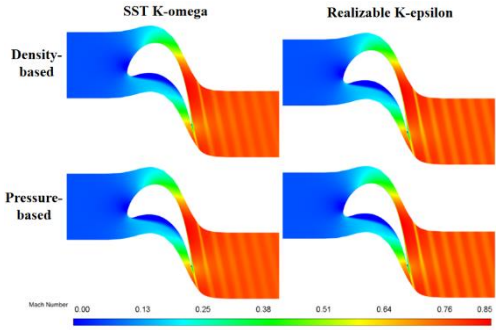

Figure 9: The Contour of Mach number of four models with exit Mach number 0.76.

A low Mach number means the kinetic energy loss is slight. Therefore, the static temperature in the trailing edge of the blade increased in a smaller area, and the distribution near the outlet is more even, as shown in Figure 10. The average temperature is higher than the case with a high Mach number. This is because the two cases with the same inlet temperature have higher Mach number with shock waves increasing more loss so that the temperature will be higher.

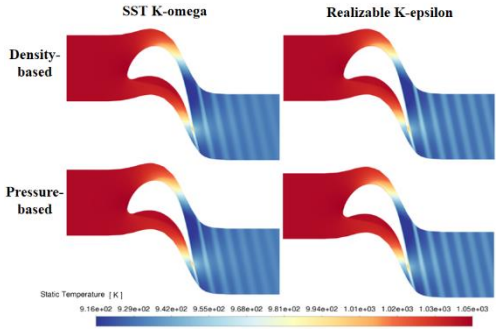

Figure 10: The static temperature of four models with exit Mach number 0.76.

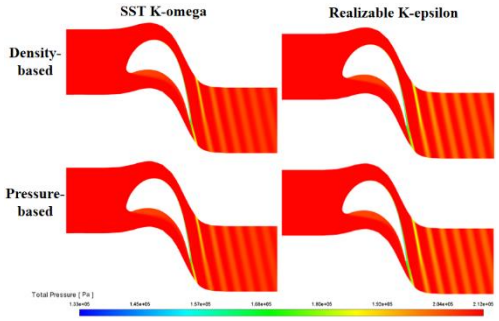

Figure 11: The Total Pressure of four models with exit Mach number 0.76.

The temperature data (Figures 7, 10) also offers information pertinent to the design of turbine blades. In a gas turbine, the turbines would endure some of the harshest operating temperatures. On top of revealing the temperatures the blades will be subject to, the temperature distribution around the blade can potentially allow the designer to measure how design changes might lead to temperature changes in the flow field and uneven distributions, if any. Furthermore, additional design measures such as cooling channels and thermal barrier coating can be incorporated to target the areas with peak temperatures.

Figure 11 shows the total pressure of four models when the outlet Mach number is 0.76. It can be seen that the total pressure drop in Figure 11 is significantly smaller than that in Figure 8. Therefore, the shock wave is one of the significant sources of loss. From this, it can be concluded that the blade curvature distribution should be in a way to minimize the effect of losses with having oblique and expansion waves in the flow.

So far, the results of the density-based and the pressure-based are not much different, and the pressure-based costs less computational time. Besides, turbulence models, SST k-ω model compared to Realizable k-ε model has more ability to accurately capture turbulent shock wave-boundary layer interaction. Therefore, the pressure-based SST k-ω model is thought to be more realistic for this study. Therefore, the computations performed and the results presented below are performed entirely with pressure based SST k-ω model.

3.2. Influence of Incidence

To study the influence of incidence on the flow around the turbine blade, different incidence angles are applied at the inlet with the same geometry 1, setting the same inlet and outlet pressure, which exit Mach number is almost 0.88, and the maximum Mach number is around 1, as shown in Figure 12. Increasing the incidence angle will bring about the translation of the low-speed stagnation regions from the blade leading edge to the pressure side and increase in inlet Mach numbers.

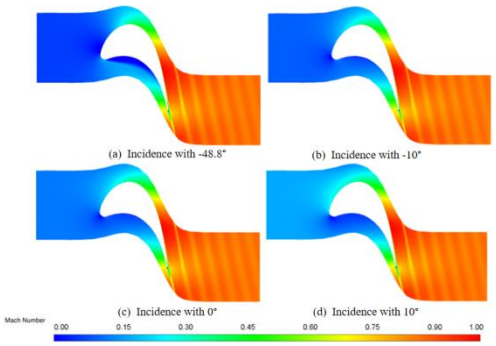

Figure 12: Contour of influence of incidence on Mach number in Geometry 1

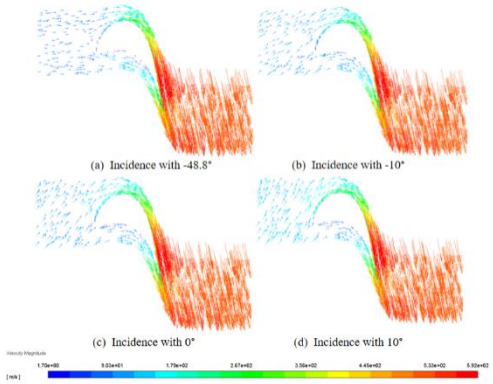

(a) Contours of velocity vectors

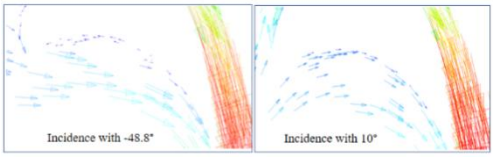

(b) Zoom-in Figures of two incidence angle

Figure 13: Contours of velocity vectors showing effect of incidence angle on the Geometry 1.

Figure 13 shows the contour of the velocity vector and zoom-in figures. Figure 13(a) compares the contour of different incidence angles on Mach number in Geometry 1. From the zoom-in figure (b), showing some specific details, there is a backflow and vortex near the pressure side boundary region when the incidence angle is -48.8º, which may cause more losses. However, as the incidence angle change to 10º, there is no reverse flow and vortex.

Isentropic Mach number and static pressure values along the blade surface normalized with total inlet pressure p_s⁄p_(0,in) are plotted against the axial distance from the leading edge of the blades (x⁄C_axial), where C_axial is the blade axial chord, is adopted to better evaluate performance due to the small numerical differences for blade profile losses, which shows in Figure 14. The small 'loop' in Figure 14 (a) when the incidence is -48º indicates negative work done by the blade from the flow before the position of 0.25. The net area enclosed by the curve can be related to the work output by the blade so that a larger one will indicate better work output. Besides, we can also know that over-expansion between the throat and trailing edge exits some diffusion, with an increase in loss. Figure 14 (b) compares the influence of different incidences on isentropic Mach number distribution. It can be seen from the Figure 14 (b) that the maximum isentropic Mach number of the four cases does not exceed 1. The blade's performance depends largely on the amount of diffusion and diffusion rate, which is also important when we further optimize the blade performance in the future.

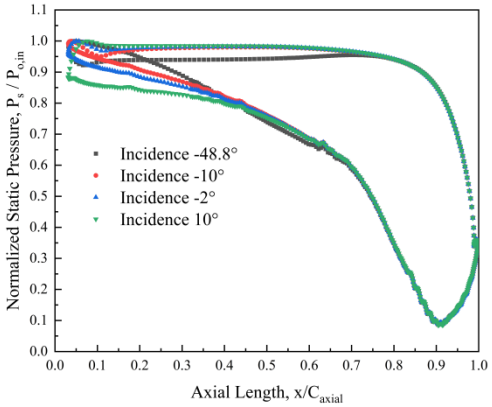

(a) Normalized Static Pressure

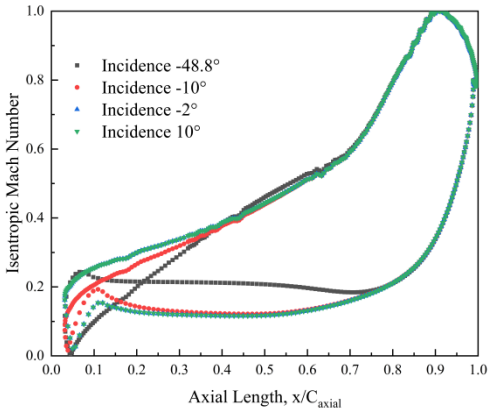

(b) Isentropic Mach Number

Figure 14: Influence of incidence on blade loading along the surface of the blade in Geometry 1.

Identifiable from Figure 14, the incidence of 10º gives the largest work output (within the studied range). This information could be incorporated either into the design of the trailing edge blade angle of the stator stage upstream of the concerned rotors or the orientation of the rotor blades to obtain the desired incidence angle.

On the other hand, gas turbines frequently operate at off-design conditions. The airflow entering each turbine stage can be far from the designed incidences at off-design conditions. A transonic or low supersonic flow coupled with a large incidence, possibly leading to a significant flow separation on the turbine blade, would pose a real challenge for turbine designers. The data obtained from incidence angle simulations can be useful for performance analysis of off-design operating conditions.

3.3. Effects of Exit Blade Angle and Incidence

Figure 15 shows the Mach number distribution of the blades in Geometries 1 and 2.

The performances of Geometry 1 and Geometry 2 with the incidence of 10º and -10º were compared to observe the influence of the modified exit blade angle on the blade performance. The results are shown in Figures 16.

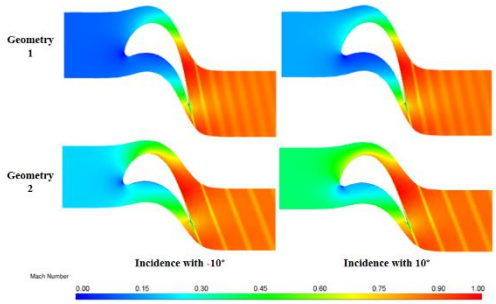

Figure 15: The Mach number distribution of the blades in Geometries 1 and 2.

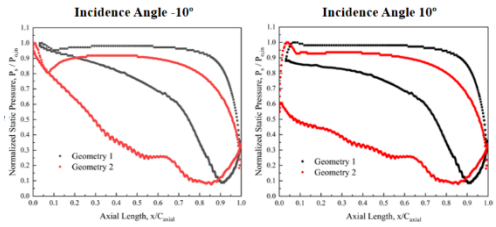

(a) Normalized Static Pressure

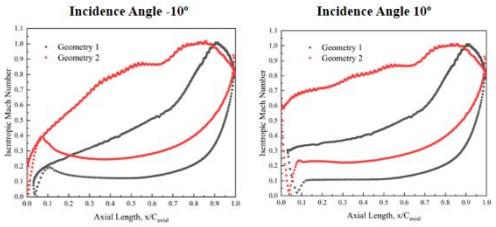

(b) Isentropic Mach Number

Figure 16: Influence of incidence on blade loading along the surface of the blade in Geometry 1 and 2.

Figure 16(a) shows the normalized static pressure distribution along the blade surface. The enclosed curve area of Geometry 2 for all studied incidence angles is bigger than those of Geometry 1.

From Figure 16(b), Geometry 2 has a smaller maximum isentropic Mach number for the same incidence angle than Geometry 1. Besides, the position of peak velocity on the suction side is earlier, so the diffusion rate is less, with a decrease in loss.

By this measurement, the performance of Geometry 2 is better than Geometry 1, which indicates that decreasing the exit blade angle has led to improving the performance of the current turbine blade.

4. Conclusion

This paper mainly focuses on applying CFD with a suitable turbulence model to evaluate turbine rotor blade performance. The results have shown the adequacy of the four RANS models – pressure and density-based Realizable k-ε and SST k-ω, in simulating the flow field trends for the Geometry blade design to a reasonable accuracy. The pressure-based SST k-ω model has been eventually picked as the model of choice due to the slightly better matching of the experimental data trends, capability to capture shock waves in the performed simulations more accurately, lower computational cost of the pressure-based solver, as well as SST k-ω model's theoretical superior ability to handle complex flows including those around turbine blades. So this paper finds a cost-effective CFD model that can predict performance trends with reasonable accuracy. It provides a more convenient and reliable method for performance evaluation of 2D turbine blade geometries.

Besides, different incidence angles are studied to see the influence on the blade performance. Within the study range, the inflow incidence angle of 10° is found to have the best performance in terms of turbine work output. Two geometries were designed by setting two different exit blade angles to observe the influence of the modified exit blade angle on the blade performance. The blade performance of Geometry 2 appears superior to Geometry 1.

Finally, Geometry 2 with an exit blade angle of 70º, coupled with the incidence angle of 10º (among the cases of incidence studied), has been shown to give the largest work output and fewer losses.

References

Lebele-Alawa B T, Hart H I, Ogaji S O T, et al. Rotor-blades' profile influence on a gas-turbine's compressor effectiveness[J]. Applied Energy, 2008, 85(6): 494-505.

Fast M, Assadi M, De S. Development and multi-utility of an ANN model for an industrial gas turbine[J]. Applied Energy, 2009, 86(1): 9-17.

Korakianitis T. Hierarchical development of three direct-design methods for two-dimensional axial-turbomachinery cascades[J]. 1993.

Korakianitis T, Papagiannidis P. Surface-curvature-distribution effects on turbine-cascade performance[C]//Turbo Expo: Power for Land, Sea, and Air. American Society of Mechanical Engineers, 1992, 78934: V001T01A044.

Korakianitis T P. Design of airfoils and cascades of airfoils[J]. AIAA journal, 1989, 27(4): 455-461.

Nemnem A F, Turner M G, Siddappaji K, et al. A smooth curvature-defined meanline section option for a general turbomachinery geometry generator[C]//Turbo Expo: Power for Land, Sea, and Air. American Society of Mechanical Engineers, 2014, 45615: V02BT39A026.

Song Y, Gu C W, Xiao Y B. Numerical and theoretical investigations concerning the continuous-surface-curvature effect in compressor blades[J]. Energies, 2014, 7(12): 8150-8177.

Mee D J, Baines N C, Oldfield M L G, et al. An examination of the contributions to loss on a transonic turbine blade in cascade[J]. 1992.

Moshizi S A, Madadi A, Kermani M J. Comparison of inviscid and viscous transonic flow field in VKI gas turbine blade cascade[J]. Alexandria Engineering Journal, 2014, 53(2): 275-280.

M. Mahmoudi, M. Ansari, Numerical investigation of turbine blade trailing edge flow ejection effects on mach number distribution of gas turbine blade surface. Using rng.k-e turbulence model[J].2005.

Corriveau D, Sjolander S A. Influence of loading distribution on the off-design performance of high-pressure turbine blades[J]. 2007. JNL/27.2.97.